Energy Transfer in Light-Adapted Photosynthetic Membranes: From Active to Saturated Photosynthesis

Francesca Fassioli,[†*] Alexandra Olaya-Castro,[‡*] Simon Scheuring,[§] James N. Sturgis,[¶] and Neil F. Johnson[‖]
[†]Clarendon Laboratory, Department of Physics, University of Oxford, Oxford, United Kingdom; [‡]Department of Physics and Astronomy, University College London, London, United Kingdom; [§]Institut Curie, Paris, France; [¶]Laboratoire d'Ingénierie des Systèmes Macromoléculaires and Institut de Microbiologie de la Méditerrannée, Centre Nationale de la Recherche Scientifique, Aix-Marseille Université, Marseille, France; and [‖]Physics Department, University of Miami, Miami, Florida

ABSTRACT In bacterial photosynthesis light-harvesting complexes, LH2 and LH1 absorb sunlight energy and deliver it to reaction centers (RCs) with extraordinarily high efficiency. Submolecular resolution images have revealed that both the LH2:LH1 ratio, and the architecture of the photosynthetic membrane itself, adapt to light intensity. We investigate the functional implications of structural adaptations in the energy transfer performance in natural in vivo low- and high-light-adapted membrane architectures of *Rhodospirillum photometricum*. A model is presented to describe excitation migration across the full range of light intensities that cover states from active photosynthesis, where all RCs are available for charge separation, to saturated photosynthesis where all RCs are unavailable. Our study outlines three key findings. First, there is a critical light-energy density, below which the low-light adapted membrane is more efficient at absorbing photons and generating a charge separation at RCs, than the high-light-adapted membrane. Second, connectivity of core complexes is similar in both membranes, suggesting that, despite different growth conditions, a preferred transfer pathway is through core-core contacts. Third, there may be minimal subareas on the membrane which, containing the same LH2:LH1 ratio, behave as minimal functional units as far as excitation transfer efficiency is concerned.

INTRODUCTION

Pigment-protein light-harvesting (LH) complexes, LH2 and LH1, transfer energy from photons to electronic excitations in the reaction centers (RCs) of purple bacteria (1–4). The special pair of bacteriochlorophylls (BChls) in the RC (5) becomes excited to its first excited singlet state, and in ~3 ps (6,7) the electron is transferred to the successive charge carriers, leading to ATP synthesis (2,8).

The issue of excitation transfer and trapping in photosynthesis has been extensively studied and modeled in the last 50 years (9–16). However, it is only until recently that submolecular-resolution images of various photosynthetic membranes have become available, revealing the structure and organization of the pigment-protein aggregates on a large spatial scale (17–21). These images show that the architecture of the photosynthetic membrane adapts to different light intensities by increasing the relative stoichiometry between the LH2 and LH1 complexes and by the appearance of LH2 paracrystalline domains under low-light conditions (19). Interestingly, despite different growth-conditions, the local arrangement of core complexes (an LH1 plus an RC) is identical in both cases, presenting two LH1s that are either adjacent or separated, at most, by one LH2.

Light adaptations are believed to increase photon capture under low light conditions and prevent burnout under high light conditions. However, their exact role in the energy transfer efficiency is not fully understood. First, very few studies have attempted to connect different membrane architectures to excitation transfer dynamics (22,23). Secondly, they have only focused on a single excitation present in the system and the regime of active photosynthesis with all RCs available for a charge separation (open state). As we show later, under continuous illumination and even under relatively high light intensities, the rate of photon capture is low enough to guarantee that there is, at most, one excitation present on the membrane. However, once there is charge separation within an RC, the special pair is in an oxidized state and/or a successive electron carrier is reduced. Depending on how fast photons arrive at the membrane, it is then plausible that some RCs are in a closed state and thus unable to perform a new charge separation (24). Therefore, an understanding of the effects of light adaptations on the dynamics of excitation transfer in photosynthetic membranes requires going beyond the active photosynthesis assumption.

In this work, we present a mathematical model to describe the energy transfer in photosynthetic membranes under continuous illumination at a given light intensity. The model allows us to explore intensity values for which photosynthesis goes from an active to a saturated regime with all RCs in their closed state. Here it is assumed that the membranes are illuminated during a time sufficiently short such that their architecture does not change in response to light. We apply our theory to natural, in vivo, low-light (LL) and high-light (HL) adapted membranes (Fig. 1) of purple bacteria *Rhodospirillum photometricum*, revealed by atomic force microscopy, which are representative membrane regions. We investigate the effects on the energy

Submitted April 22, 2009, and accepted for publication August 3, 2009.

*Correspondence: f.fassioli1@physics.ox.ac.uk or a.olaya@ucl.ac.uk

Editor: Lukas K. Tamm.

0006-3495/09/11/2464/10 $2.00

doi: 10.1016/j.bpj.2009.08.033

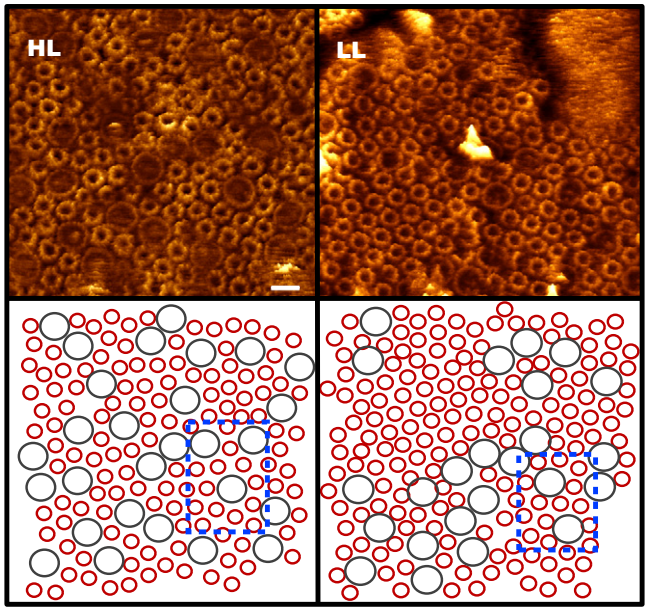

FIGURE 1 (*Top*) AFM images of the light harvesting LH1 (*large ring*) and LH2 (*small ring*) photosynthetic complexes, in a high-light (*HL*) and a low-light (*LL*) adapted membrane of *Rsp. photometricum* (originally published in (19)). Scale bar is 10 nm. (*Bottom left*) LH network based on AFM images of HL-adapted membrane grown at an intensity $I = 100$ W/m^2, with LH2:LH1 = 4.64. (*Bottom right*) LH network of a LL-adapted membrane grown at an intensity $I = 10$ W/m^2, with LH2:LH1 = 7.04. Notice that in the LL membrane there is an area containing LH2-only arrays.

transfer of the light intensity and RC reopening time, i.e., the time taken for an RC to pass from its closed to open state. We first focus on the quantum yield, which is the efficiency of excitation trapping at the RC, and we introduce the quantification of the overall efficiency of capturing a photon and delivering it to the RC for charge separation. Then, we investigate the connectivity of core complexes. Finally, we compare the membrane's performance to that of a subarea with the same LH2:LH1 ratio.

Relevant timescales under continuous illumination

We start by discussing the timescales for energy capture, the excitation lifetime, and the reopening of the RC. The rate at which an LH2 or LH1 gets excited by absorption of incident photons depends upon their wavelength-dependent absorption cross-section and the frequency spectrum. The rate R of photon capture in a membrane is given by $R = \int d\lambda\, n(\lambda)\, \sigma(\lambda)$, where $n(\lambda)$ is the spectral photon density and $\sigma(\lambda)$ is the membrane's total absorption cross section at wavelength λ. In *Rsp. photometricum*, each LH2 has nine subunits consisting of two carotenoids, one BChl B800, and two BChls B850, whereas the LH1 has 16 subunits with one carotenoid and two BChls B875 (19,25,26). For simplicity, we assume that the membrane is illuminated by a monochromatic source of 850 nm. The only relevant absorption cross section at this wavelength is that of the BChls B850 and B875. The extinction coefficients of B850 and B875 at 850 nm are 170 and 55 (mM cm)$^{-1}$ (27), respectively, which translate into an absorption cross section (28) of $\sigma_2 = 117$ Å^2 for the LH2 and $\sigma_1 = 67.29$ Å^2 for the LH1. Therefore, the rate of photon capture at an intensity I reduces to $R = I\sigma/h\nu$, where $\sigma = N_1\sigma_1 + N_2\sigma_2$ and $N_{1(2)}$ is the total number of LH1(2) complexes. For example, at an intensity of $I = 100$ W/m^2, the HL- and LL-adapted membranes (Fig. 1, *bottom*) capture photons at a rate of $R_H = 73{,}050$ photons/s and $R_L = 91{,}400$ photons/s, respectively, which gives a mean period of excitation of $\sim R^{-1}$ $\sim 10^{-5}$ s. As the average excitation lifetime is hundreds of picoseconds, there is, at most, one excitation at a time on the membrane.

The second relevant timescale is the reopening time of the RC, which depends on the ambient redox potential (electron availability), and thus will be modified by environmental conditions such as oxygen concentration (29–33). Estimates of the RC turnover time under continuous illumination in *Rhodopseudomonas sphaeroides* vary considerably, depending on the ambient redox potential, but is ~1 ms/e under oxidizing conditions (30,31). However, in *Phaeospirillum molischianum*, which has a similar membrane architecture to *Rsp. photometricum*, the turnover rate is much slower than in *R. sphaeroides* and limited to ~40 e/s (34). This gives an average RC reopening time of 25 ms. Hence depending on light intensity, some RCs will still be closed from earlier charge separations when a new excitation is created in an LH. Borisov et al. (35) investigates experimentally the kinetics of BChl luminescence in *Rhodospirillum rubrum* and *R. sphaeroides*, as a function of light intensity from active to saturated photosynthesis. Note that the RCs in a closed state not only are unable to generate a stable charge separation, they are also strong quenchers of excitations (24). Although the average fluorescence lifetime in membranes lacking RCs is ~1000 ps (24,36), the lifetime is significantly lower in membranes where all RCs are closed, with values at ~200 ps (24,35). Moreover, the ratio between fluorescence in saturated and active photosynthesis is only 2–3 (24,35), supporting nonfluorescent excitation dissipation at the RC.

Energy transfer from active to saturated photosynthesis

In active photosynthesis, the dynamics of the excitation transfer on the membrane is usually described in terms of a probability master equation for a single excitation hopping from site to site (37). We now explain how the separation of timescales of photon capture, excitation lifetime, and RC reopening time, allow the same formalism to be applied, hence the excitation transfer under continuous illumination can be described in terms of a random migration of a single excitation in a membrane with an effective fraction of closed state RCs.

The photosynthetic membrane is modeled as a network of N sites corresponding to an LH2, an LH1, or an RC (at the

center of each LH1) (Fig. 1, *bottom*). The process of energy capture and transfer through such LH network involves three important steps:

1. An LH complex becomes excited with an average period of $P = R^{-1}$. A given LH2(1) is chosen with probability $\sigma_{2(1)}/\sigma$.
2. The excitation executes a hop through an incoherent Förster mechanism from site to site until it either dissipates, or is used for charge separation at an open RC.
3. After charge separation has occurred at an RC, this RC remains in a closed state for a time t_{block}, during which it is unable to perform a new charge separation. In its closed state, the RC becomes a strong quencher of excitations, increasing its dissipation rate (24).

The number of RCs in a closed state will depend on the light intensity and t_{block}, and, in principle, will vary in time. However, as shown in Fig. 2, the system reaches the average value of closed RCs, N_{block}, in a timescale much shorter than the total evolution time, and then fluctuates around this value. Hence, to compute performance quantities that are averages in time, the energy transfer on the membrane at a particular intensity can be seen as a single excitation migrating on a LH network with an average number of RCs unavailable. Therefore, the energy transfer can be described by a master equation of probability, and the energy features can be expressed as functions of N_{block}.

Master equation

The excitation transfer is governed by the different probability rates. We define W_{nm} as the rate of excitation transfer from sites m to n. The dissipation rate k_{diss} is assumed equal at all sites, except at closed RCs where the rate is $k^*_{\text{diss}} >>$ k_{diss}. The charge separation rate at an open RC is denoted by k_{cs}. Letting p_{m} be the probability that site m is excited, yields

$$\frac{dp_{\text{m}}}{dt} = \sum_{\text{n}} K_{\text{mn}} p_{\text{n}}, \tag{1}$$

where

$$K_{\text{mn}} = W_{\text{mn}} - \delta_{\text{mn}}\left(\sum_{\text{l}} W_{\text{ln}} + \delta_{\text{n,RC}^{\text{o}}} k_{\text{cs}}\right) - \delta_{\text{mn}}\left(k_{\text{diss}}(1 - \delta_{\text{n,RC}^{\text{c}}}) + k_{\text{diss}^*}\delta_{\text{n,RC}^{\text{c}}}\right) \tag{2}$$

and RC^{o} and RC^{c} denote an open and closed RC, respectively. In matrix form, Eq. 1 reduces to $|\dot{p}(t)\rangle = K|p(t)\rangle$, where $|p(t)\rangle$ is an N-component vector whose m^{th} component is p_{m} and K is the transfer rate matrix with elements K_{mn}. The solution is simply $|p(t)\rangle = e^{\text{Kt}}|p(0)\rangle$.

As a first approximation, we take the transfer rates W_{mn} as the inverse of the excitation transfer times computed (22) or measured (2,38,39) for purple bacteria. In particular, for the LH2 → LH2, LH1 → LH1, and LH1 → LH2 transfer rates, we have used the transfer times derived through quantum chemical calculations in Ritz et al. (22) and the corresponding values are $(10\ \text{ps})^{-1}$, $(20\ \text{ps})^{-1}$, and $(15.5\ \text{ps})^{-1}$, respectively. The transfer rates LH2 → LH1, LH1 → RC, and RC → LH1, have been taken from the experimentally measured times and are $(3.3.\ \text{ps})^{-1}$ (38), $(25\ \text{ps})^{-1}$ (2), and $(8\ \text{ps})^{-1}$ (39), respectively. Since the Förster transfer rates between BChls separated by a distance d decay as $\sim 1/d^6$ (22), the transfer rates between non-nearest neighbors will be assumed negligible. The charge separation rate is taken to be $k_{\text{cs}} = (3\ \text{ps})^{-1}$ (7), and the dissipation rate is taken as the inverse of the singlet excited state lifetime of BChl (1 ns), $k_{\text{diss}} = 1/1000\ \text{ps}^{-1}$ (24,36). For a closed RC, there has been no precise dissipation rate reported, to our knowledge. In Borisov et al. (35) it is shown that the average fluorescence lifetime for *R. sphaeroides* in active photosynthesis is 50–70 ps while in the saturated regime it is ~200 ps. The former approximates the fluorescence lifetime measured for our HL-adapted membrane. Hence, we choose a value of $k^*_{\text{diss}} = (30\ \text{ps})^{-1}$ such that the average fluorescence lifetime of the HL-adapted membrane matches that of Borisov et al. (35) for saturated photosynthesis.

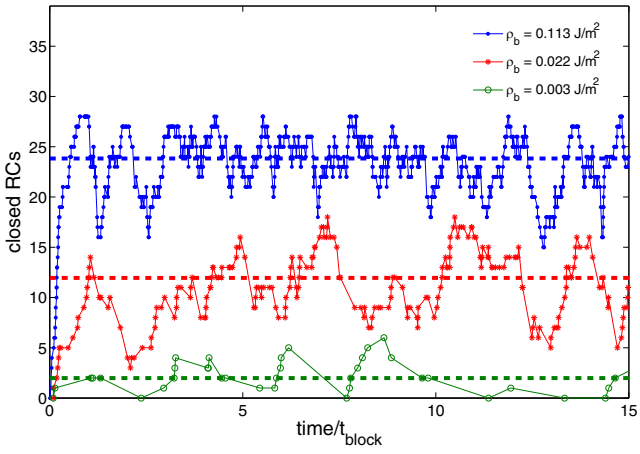

FIGURE 2 Number of RCs in a closed state as a function of time given by the continuous illumination simulation (HL membrane). Horizontal lines show the average number of closed RCs, N_{block}, for a particular ρ_{b}. These averages indeed satisfy Eq. 5, i.e., $\rho_{\text{b}} \times \sigma/h\nu = N_{\text{block}}/\eta$, and the performance measures obtained through the master equation with the average N_{block}, are in very good agreement with those obtained with the continuous illumination simulation.

Performance measures

The optimality and robustness of energy transfer in photosynthetic systems are usually quantified through performance measures that are integrated success probability densities (37). We focus on four measures:

1. The quantum yield η_{j}, which is the probability that an excitation initially present on complex j, i.e., $|p(0)\rangle = |j\rangle$, is used for charge separation.
2. The excitation lifetime, τ_{j}, which is the average time before it is dissipated or trapped at an RC.

3. The fluorescence yield, ϕ_j, which is given by the probability that the excitation is dissipated fluorescently by any of the LH complexes.
4. The fluorescence lifetime, τ_{ϕ_j}, which is the average lifetime of an excitation that is lost by fluorescence.

Measures 3 and 4 are of particular interest, as they will allow us to compare our results with available experimental results (35).

Define $\omega(t)\,dt$ as the probability that in $[t, t+dt)$ the excitation is lost from the system either by charge separation or dissipation. Similarly, $\omega_{cs}(t)$ and $\omega_\phi(t)$ are the probability densities that the excitation is used for charge separation and that it is dissipated by an LH, respectively. Then our performance measures are given by

$$\begin{aligned} \eta_j &= \int_0^\infty dt\,\omega_{cs}(t), \phi_j \;\; = \int_0^\infty dt\,\omega_\phi(t) \\ \tau_j &= \int_0^\infty dt\,t\,\omega(t),\; \tau_{\phi_j} = \frac{1}{\phi_j}\int_0^\infty dt\,t\,\omega_\phi(t) \end{aligned}, \tag{3}$$

where $\omega_{cs}(t) = k_{cs}\langle RC^o|p(t)\rangle$ and $\omega_\phi(t) = k_{diss}\langle LH|p(t)\rangle$, with $|RC^o\rangle$ a vector with the value 1 at a site that represents an open RC, and the value 0 elsewhere. Similarly for $|LH\rangle$. Let now $s(t)$ be the survival probability, i.e., the probability that at time t the excitation remains in the system, i.e., $s(t) = \langle 1|p(t)\rangle$. Then $\omega(t)$ is given by $-ds(t)/dt$, and the integrals in Eq. 3 become

$$\begin{aligned} \eta_j &= -k_{cs}\langle RC^o|K^{-1}|j\rangle,\;\; \phi_j \;\; = -k_{diss}\langle LH|K^{-1}|j\rangle \\ \tau_j &= -\langle 1|K^{-1}|j\rangle,\; \tau_{\phi_j} = -\frac{\langle LH|K^{-2}|j\rangle}{\langle LH|K^{-1}|j\rangle} \end{aligned}. \tag{4}$$

RESULTS AND DISCUSSION

We use both the master equation formalism described above and a random walk simulation (see Appendix) to obtain the excitation dynamics on the membranes represented by the networks in Fig. 1 (*bottom*). Such membranes are a section of a larger chromatophore membrane, hence to avoid border effects we apply periodic boundary conditions. When using a master equation, we first calculate the quantities of interest as a function of the average number of closed RCs, N_{block}. To do this, we randomly choose an initial state $|j\rangle$ and the N_{block} RCs in a closed state to determine the rate matrix K (Eq. 2) and calculate from Eq. 4 the values of η_j, ϕ_j, τ_j, and τ_{ϕ_j}. We repeat the process 10^4 times, and obtain $\eta = \langle\eta_j\rangle$, $\phi = \langle\phi_j\rangle$, $\tau = \langle\tau_j\rangle$ and $\tau_\phi = \langle\tau_{\phi_j}\rangle$ as the average over the different initial configurations, all with the same value for N_{block}.

In principle, N_{block} depends on the particular value chosen for the RC reopening time and the light intensity. However, t_{block} may well vary from membrane to membrane and with intensity. To avoid our results being dependent on a particular value assumed for this time, we express the performance measures as functions of the quantity $\rho_b \equiv$ Intensity $\times\, t_{block}$, which is the energy density available to the membrane during the time interval t_{block}. To find a quantitative relation between N_{block} and ρ_b, note that the former is given by the number of charge separations N_{cs} during the time interval an RC remains closed, i.e., $N_{block} = t_{block} \times N_{cs}/\Delta t$. The number of charge separations per unit time is related to the quantum yield as $N_{cs}/\Delta t = R \times \eta$. Substituting the latter relation into the expression for N_{block} and replacing $R = I\sigma/h\nu$ yields

$$\rho_b \times \frac{\sigma}{h\nu} = \frac{N_{block}}{\eta}. \tag{5}$$

From the master equation approach, we have η as a function of N_{block}, i.e., $\eta(N_{block})$. By substituting η and its corresponding N_{block} in Eq. 5, we obtain the value of ρ_b corresponding to a particular choice of N_{block}. The advantages of using ρ_b is that it shows explicitly the combined effect of different reopening times and intensities, and makes our results only dependent on measured transfer rates and structural membrane parameters, that is, the total absorption cross-section σ.

Overall performance

The only available experimental measure for the types of membranes we are considering is the LH2 fluorescence yield ϕ_2, i.e., the probability that the excitation is dissipated in an LH2 when all RCs are in an open state. We calculate $\phi_2 = \langle\phi_{2j}\rangle$, with $\phi_{2j} = -k_{diss}\langle LH2|K^{-1}|j\rangle$ (analogously as ϕ_j in Eq. 4). We find $\phi_2^H = 0.034$ and $\phi_2^L = 0.057$ for the high- and low-light adapted membranes, which are in good agreement with approximate experimental values of $\phi_2^H = 0.020$ and $\phi_2^L = 0.055$ (C. Mascle-Allemand and J. N. Sturgis, unpublished).

We now calculate the quantum yield η, fluorescence yield ϕ, lifetime τ, and fluorescence lifetime τ_ϕ for the HL- and LL-adapted membranes as a function of ρ_b, which is the energy density during the time interval t_{block}. Results are shown in Fig. 3. The increase in ϕ and τ_ϕ with ρ_b compares qualitatively with the behavior reported in Borisov et al. (35). We find a ratio between fluorescence in saturated (ϕ_{sat}) and active (ϕ_{act}) photosynthesis of 2.84 (HL membrane) and 2.70 (LL membrane), in good agreement with the observed 2–3 range (24,35). Comparing values for HL and LL membranes, we find at a given ρ_b that the HL-adapted membrane always has a greater quantum yield than the LL-adapted one. This is an expected result if we consider the following. First, in the limit $\rho_b \to 0$ (active photosynthesis), the HL membrane has a higher quantum yield than the LL membrane, because its larger RC fraction makes it more likely for an excitation to find an RC for charge separation before dissipating (23). Second, for a given light intensity I, the frequency at which an LH is excited is higher for the LL membrane than for the HL membrane—hence, if reopening times are comparable in the two membranes, we

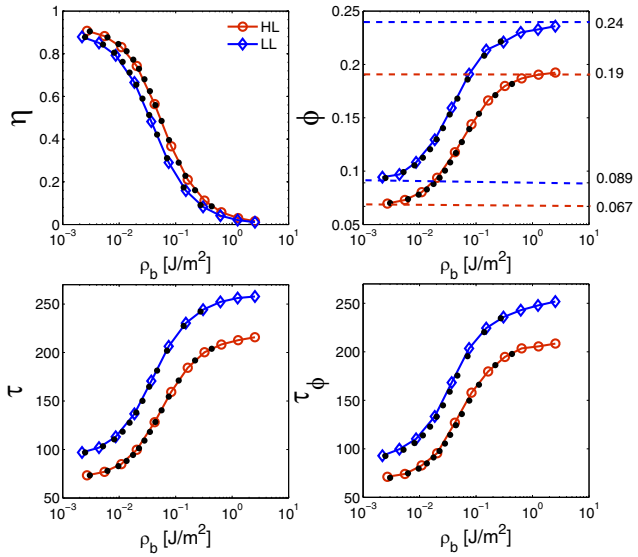

FIGURE 3 Comparison between HL (○, random walk) and LL (◇, random walk) adapted membranes. Master equation results are represented by solid circles. Quantum yield η (*top left*), fluorescence yield ϕ (*top right*), lifetime τ (*bottom left*), and fluorescence lifetime τ_ϕ (*bottom right*) as a function of ρ_b = Intensity × t_{block}. The values τ and τ_ϕ are in units of picoseconds. Note that $\phi_{sat}/\phi_{act} = 0.19/0.067 = 2.84$ for the HL membrane and $\phi_{sat}/\phi_{act} = 0.24/0.089 = 2.70$ for the LL membrane.

expect η to decay faster in the LL membrane, reaching the regime of saturated photosynthesis first.

How the quantum yield depends on the initial position of the excitation is an interesting matter. In particular, it provides insight into how the excitation diffusion is affected by the LH2-only domains in the LL membrane. To investigate this point, the quantum yield for the LL membrane in active photosynthesis has been calculated as a function of the initial state with the excitation initially located at an LH2 complex. The lowest quantum yield value of 0.89 is found when the excitation is initially at the LH2 in the middle of the paracrystalline zone (see Fig. 1, *bottom right*), and the maximum value of ~0.92 for initial states with the excitation localized at an LH2 next to an LH1. The performance measures shown in Fig. 3 are averages over different initial configurations with an overall quantum yield of 0.91. Therefore, the average quantum efficiency is not drastically affected by the paracrystalline zone. In contrast, it has been suggested that the presence of these quasi-static large areas have a strong effect in the diffusion of electron carriers (40).

Optimized efficiency

We define the efficiency as the probability that an incident photon is used for charge separation, i.e., Efficiency $= N_{cs}/N_\gamma$, where N_γ is the number of incident photons. Unlike the quantum yield, which measures the probability of charge separation conditioned on an excitation being already present in the system, the efficiency also takes into account the probability that a photon excites an LH aggregate. The efficiency is a key quantity since, for a given intensity, it is directly proportional to the number of charge separations per unit time per unit area, and therefore an indicator of the system's ability to produce energy.

The efficiency is obtained in a straightforward way from the quantum yield. The number of incident photons per unit time is given by $N_\gamma/\Delta t = R \times A/\sigma$, with A the total area of the membrane, and $N_{cs}/\Delta t = R \times \eta$. Hence, we obtain

$$\text{Efficiency} = \eta \times \sigma/A. \tag{6}$$

Our results (Fig. 4) show that there is a critical energy density ρ_b^c below which the LL membrane is more efficient than the HL membrane. Even if the LL membrane is always ''worse'' at converting an excitation into a charge separation (quantified by η), the key point is that the LL membrane is ''better'' at capturing a photon, i.e., it is ''better'' at actually receiving an excitation. Assuming the same t_{block} for both membranes, the crossover occurs at $I = 0.3$ W/m^2 for $t_{block} = 25$ ms, and at $I = 7.47$ W/m^2 for $t_{block} = 1$ ms. These calculations assume illumination by light centered at 850 nm. To obtain the same rates of excitation with white light we would need approximately four times such intensity values (41), and even higher intensities when the light source is an incandescent light (such as when the membranes were grown). But how far can one exploit the strategy of enhancing the effective cross-sectional area for absorption by adding LH2 domains? In particular, will there always be a crossover point in Fig. 4 or is the loss in quantum yield eventually too much? A necessary condition for the crossover to exist is that when $\rho_b \to 0$ the LL membrane efficiency is greater than the efficiency of the HL membrane. Therefore, we need to determine how the efficiency in the active

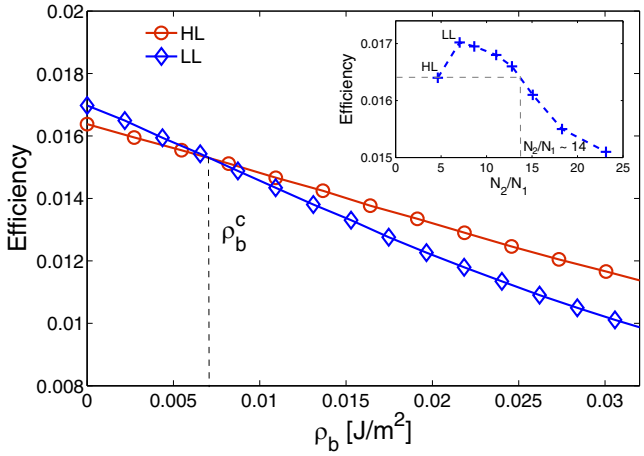

FIGURE 4 Efficiency as a function of ρ_b = Intensity × t_{block} for the HL (○) and LL (◇) adapted membrane. $\sigma/A \simeq 0.0176$ and $\sigma/A \simeq 0.0187$ for the HL and LL membranes, respectively. (*Inset*) Efficiency in the limit $\rho_b \to 0$ as a function of different LH2:LH1 ratios. Over a ratio of LH2:LH1 ~14, the crossing in the efficiency curves vanishes, i.e., the HL membrane is more efficient independent of ρ_b.

photosynthesis regime varies with LH2:LH1. To address this issue, we created networks of different LH2:LH1 ratios by replacing a number of LH1 by LH2 complexes in the original LL membrane network. We have computed the quantum yield and corresponding efficiency of the modified networks. Results are shown in the inset in Fig. 4, and they indicate that for LH2:LH1 ratios >~14, there is no longer a crossover; that is, the HL membrane is more efficient for all intensities. We note, however, that for native membranes the ratio values reported in the literature are between 3 and 10 (26,42). This may suggest that natural systems may, in general, exhibit such crossover.

Core-core connectivity

In both high- and low-light adapted membranes of *Rsp. photometricum*, the local environment of core complexes is maintained such that two LH1 complexes tend to be found in close contact or separated by one LH2 at most. It has been suggested that this arrangement may be of importance when an RC is in a closed state, since it can allow an excitation that has arrived to a closed core to be transferred to the neighboring LH1, thereby increasing the chances of the excitation finding an open RC (19,23). The relation between the state of the RC and the excitation diffusion has been investigated in early theoretical models for photosystem II (43–45). Şener et al. (23) have reported that in chromatophores of *R. sphaeroides*, and in an active photosynthesis regime, an excitation that has been detrapped from an RC is most likely to be trapped within the same dimeric core complex. It has also been suggested that LH1-LH1 aggregation may be favorable for quinone diffusion (40), thus reducing the time t_{block} and therefore increasing the yield as a function of light intensity. To investigate the effect of such preferential arrangement on the energy transfer performance when some RCs are in their closed state, we focus on two limiting situations: 1), only a single RC is closed; and 2), all RCs are closed. We first calculate the probability that an excitation in the single closed RC can be detrapped from it and used for charge separation in any given open RC. As illustrated in Fig. 5 (*top*), the excitation will most likely be used for charge separation in one of the RCs in close contact. This characteristic remains in both HL and LL membranes, and the overall probability of charge separation at any RC is 0.69 and 0.68, respectively. This indicates that in both membranes, a preferred pathway of excitation transfer is through neighboring core complexes. We estimate the connectivity between core complexes, by calculating the connectivity parameter J (45,46).

In Fig. 5 (*bottom*) we plot the normalized relative fluorescence yield, $\phi_v = (\phi - \phi_{act})/(\phi_{sat} - \phi_{act})$, as a function of the fraction of closed RCs (c), where the dotted line is a fit to the function $\phi_v = c/(1 + J(1 - c))$. We find similar connectivity parameters for both membranes, with values of $J = 1.7$ and $J = 1.6$ for the HL and LL, respectively. The significance of

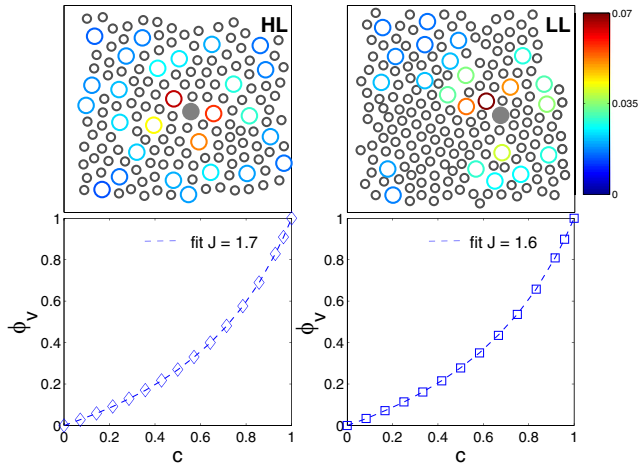

FIGURE 5 (*Top*) Probability that an excitation that arrives to the RC in the closed state, denoted by a solid circle, is detrapped and used for charge separation in a given open RC. (*Bottom*) Normalized relative fluorescence yield $\phi_v = (\phi - \phi_{act})/(\phi_{sat} - \phi_{act})$ as a function of the fraction of closed RCs (c). The line is a fit to $\phi_v = c/(1 + J(1 - c))$.

J is that $J + 1$ can be interpreted as the approximate number of RCs that an excitation visits, on average, when all RCs are in a closed state (45,46). Therefore we can estimate that in the saturated regime, the excitation visits, on average, 2.7 and 2.6 RCs in the HL and LL membranes, respectively, before being dissipated. We have independently computed this average in the random walk simulation and found values of 3.1 and 2.8 for the HL and LL membranes, respectively, in good agreement with the aforementioned significance of J. The value of $J + 1$ ~3 for both membranes suggests again that the local organization of core complexes (which remains independent of the membranes' growth condition) plays an important role in energy transfer by providing a pathway where excitation is more likely to be trapped. Hence, core connectivity reduces energy loss and protects the cell from being damaged. The RCs also quench fluorescence dissipation. Indeed, an arriving excitation at a closed RC may be lost as heat or fluorescence and/or eventually form radicals. Radicals in the cells may, in turn, damage the DNA and cause mutations.

Minimal functional unit

We now investigate the effect of the membrane's size on the energy transfer properties. In particular, we focus on the performance of a minimal membrane subarea containing the fewest possible LH1s, such that both the LH2:LH1 ratio and the typical local core environment observed in the larger membrane are maintained. Fig. 6 compares the performance measures between the larger membrane and the dotted subarea for the HL and LL membranes (Fig. 1, *bottom*). Periodic boundary conditions have been applied. Remarkably, the quantum yield of the subarea is very similar to that of the larger membrane. The other performance quantities, i.e., fluorescence yield, excitation lifetime, and fluorescence

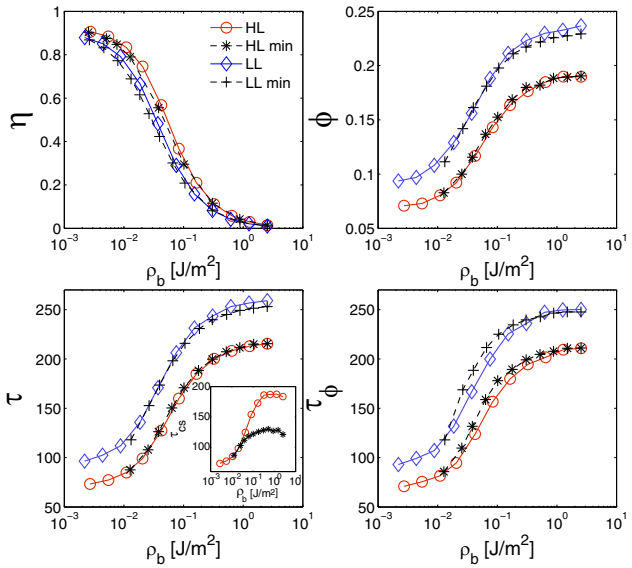

FIGURE 6 Comparison between the larger membrane and the indicated subarea (Fig. 1, *bottom*) for the HL and the LL membranes. Quantum yield η, fluorescence yield ϕ, lifetime τ, and fluorescence lifetime τ_ϕ as a function of ρ_b = Intensity $\times$ t_{block}. (*Inset*) Charge separation time τ_{cs} for the HL membrane and its corresponding subarea. The valuesτ, τ_ϕ, and τ_{cs} are in units of picoseconds. We only show results obtained from the random walk simulation: In a membrane containing only a few RCs, any variation on the number of closed RCs significantly alters the energy transfer, and therefore the master equation formalism is not appropriate.

lifetime, also compare very well—except for the latter at intermediate intensities. The striking similarities between the behavior of large and small membrane structures suggest that, as far as energy transfer efficiency is concerned, the minimal subarea could behave as a minimal functional unit. Indeed, the quantum yield is an emergent property of the whole molecular assembly. Hence, our finding seems to highlight the necessary conditions under which this emergent property would appear. We recognize, however, that the long-range connectivity of the subarea with the rest of the membrane can affect other diffusion characteristics. To illustrate this point, Fig. 6 (*inset*) shows the average charge separation time in the HL membrane (τ_{cs}). As expected, this average trapping time exhibits different behavior for the large and small areas as ρ_b increases. The reason is that τ_{cs} tends to the limit when only one RC is available. Since the small area has fewer RCs than the larger area, the excitation will arrive sooner to the available open RC in the former than in the latter. An extended study of the conditions in which the similarity between large and small areas will break, and in general, of the role of short- and long-range connectivity in the excitation diffusion properties on the membranes, is beyond the scope of this article, and will be presented elsewhere.

We finally would like to discuss the validity of our results for other species and/or as the parameters and assumptions of the model are changed. Unlike many other strains, the chromatic adaptation of *Rsp. photometricum* does not include producing spectrally distinct peripheral antennae (19). However, for species in which such adaptations occur, the model here described should be modified to include different LH excitation and intercomplex hopping rates for the different membranes. We have investigated the effects of considering different transfer rates and found that our results hold for a wide range of values in the parameter space, as long as the separation of timescales of excitation transfer/trapping in the RC and dissipation remain. For example, there is no significant change in the predicted crossing point in Fig. 4 if a faster LH1 → LH1 transfer rate, of the order of the LH2 → LH2 transfer rate, is assumed. We find that the position of such a crossing point is sensitive to the LH1 → RC rate and the dissipation rate of a closed RC. A slower LH1 → RC rate of $(41\ \text{ps})^{-1}$ (as reported in (47)) implies lower efficiency values at lower energy densities and slower decay at higher energy densities. This results in a shift of the crossing point of the HL and LL efficiency curves to approximately twice the reported value. On the contrary, if a larger dissipation rate at closed RCs is considered, $k^*_{diss} = (12\ \text{ps})^{-1}$, the efficiency decays faster as a function of energy density and the crossover in this case occurs at a lower energy density of $\rho_b^c = 0.0055\ \text{J/m}^2$. The validity of our calculations and model rely on the fact that for the intensities considered, the separation of timescales between mean period of excitation and excitation lifetime is large enough to guarantee that the probability of finding more than one excitation at a time is very low. However, under high enough intensities, singlet-singlet annihilation may occur, and the triplet states of the bacteriochlorophylls start to accumulate as well, eventually leading to singlet-triplet annihilation. Such nonlinear effects have not been analyzed here and are left for an extension of our study.

Outlook

Understanding how natural photosynthetic systems make efficient use of sunlight energy, is a fundamental step toward the development of bio-inspired artificial photosynthetic devices. Indeed, the lessons learned from Nature may be general and then of crucial importance for technical applications. In this work, we have presented a model to study the energy transfer in high- and low-light adapted membranes of *Rsp. photometricum* under continuous illumination. The differences between the two membrane architectures in terms of efficiency as a function of the intensity of incident light have been quantified and explained. These differences seem to indicate that structural adaptations guarantee that the overall efficiency of both capturing and transferring excitation to an RC as a function of intensity presents a crossover, determining the domain of intensities for which each membrane has a better performance. Our results also suggest the possibility that these supramolecular structures have subregions which, containing the same LH2:LH1 ratio and

local core-core contacts as the larger membrane area, behave as minimal functional units having the same quantum yield as the larger molecular assembly. In general, our results highlight relations between structural optimization and efficient light-to-charge conversion, giving insight into the open question concerning the relation between ecology and energy capture and transfer.

The theoretical framework presented here can be applied to a large variety of light-harvesting architectures. In particular, it is timely and relevant to the study of hybrid photosynthetic units with variable LH2:LH1 ratio (48) as well as to the recent advances in nanoscale patterning of LH2, where spatial control in the assembly of functional LH2 complexes has been achieved (49).

APPENDIX

Continuous illumination simulation

As explained under section Energy Transfer from Active to Saturated Photosynthesis, due to the separation of timescales of photon capture by the membrane and excitation lifetime, we can safely assume that there is, at most, one excitation on the membrane. This assumption is even valid at the upper limit of the energy density $\rho_b = \text{Intensity} \times t_{block} \sim 2.5\ \text{J/m}^2$, which for $t_{block} \sim 1$ ms translates into an intensity of $I = 2.5\ \text{kW/m}^2$. At this intensity, the average period of photon capture, P, for example in the LL membrane, is $P \sim 400$ ns. We assume that the photon capture events are independent of each other, and therefore the time interval T between successive excitations is obtained through an exponential probability density function $f(T) = e^{-T/P}/P$. The probability that the time interval between successive excitations is, therefore, less than the lifetime of the excitation ($\tau \sim 200$ ps) is given by $\int_0^\tau f(T)dT$, and for $P \sim 400$ ns this probability is only $\sim 5 \times 10^{-4}$. Hence, even at high intensities, the probability of two excitations coinciding on the membrane is negligible.

With an average period P, the membrane is excited N_{exc} times. We first determine from the distribution $f(T)$ the times $\{t_i\}$, $i = 1 \ldots N_{exc}$, at which the i^{th} excitation is created on the membrane. For good statistics we take $N_{exc} = 10^5$.

For each of the $i = 1 \ldots N_{exc}$ excitation events, the following cycle is carried out:

Step 1. A single LH complex on the membrane is excited: the probability that a given LH2(1) is chosen is $\sigma_{2(1)}/\sigma$.

Step 2. A random walk simulation (under Updating Rules, below) for the excitation created in Step 1 is performed until
1), the excitation dissipates; or
2), the excitation is used for charge separation at an open RC.

Step 3. If the excitation in Step 2 is used for charge separation, then the corresponding RC remains blocked for a time t_{block}. This is implemented by having the RC in the closed state for the following excitations until the n^{th} one is created, where n is obtained by finding the minimum value of n such that $t_n > t_i + t_{block}$. Therefore, the states of the RCs during the random walk of the excitation on the membrane in Step 2 remain unaltered.

Random walk simulation

First, we explain the probabilities that will govern the random walk simulation of the excitation in Step 2.

During a time step, Δt, the excitation can either stay on the same site or a jump event can happen. A jump accounts for any possible event: transfer of the excitation to another site, dissipation, or charge separation. The probability of a jump at the site j of the excitation during a time step, $p^j_{jump}(\Delta t)$, is obtained from $p^j_{jump}(\Delta t) = 1 - p^j_{no\ jump}(\Delta t)$. The probability of no jump is given by

$$p^j_{no\ jump}(t + \Delta t) = \lim_{dt \to 0} \left(1 - K_j dt\right)^{\Delta t/dt} = \exp\left[-K_j \Delta t\right] \tag{7}$$

with

$$K_j = k_{diss}\left(1 - \delta_{j,RC^c}\right) + k_{diss^*}\delta_{j,RC^c} + k_{cs}\delta_{j,RC^o} + \sum_{i \neq j} W_{ij}, \tag{8}$$

and consequently, the jump probability is

$$p^j_{jump}(\Delta t) = 1 - \exp\left[-K_j \Delta t\right]. \tag{9}$$

Note that as the states of the RC vary from one excitation to another, the jump probabilities determined by K_j will vary from excitation to excitation as well, but as mentioned earlier, will remain constant for a given excitation. To ensure that between t and $t + \Delta t$ there is at most one event, Eq. 9 implies that the time step Δt has to be chosen such that $\Delta t << 1/K_j$, so that the probability of jump is very small, i.e., $p^j_{jump}(t + \Delta t) << 1$. For this reason we use a time step of $\Delta t = 0.01$ ps.

Updating rules

The following are the updating rules for the random walk simulation in Step 2.

At each time step Δt:

Step 2.1. We find the site "j" at which the excitation is located.

Step 2.2. A jump occurs with probability p^j_{jump} (Eq. 9).

Step 2.3. If the decision on Step 2.2 was that no jump occurs, we go to Step 2.1. Otherwise, we go to Step 2.4.

Step 2.4. If a jump event happens, the excitation will either:
1), dissipate with probability k_{diss}
2), be used in charge separation at an open RC with probability k_{cs}; or
3), migrate to a neighboring site "i," with probability W_{ij} normalized over K_j.

Step 2.5. If the excitation migrates to a different site, we update the position of the excitation and go to Step 2.1.

Step 2.6. If charge separation takes place, we record the site at which this happened and the loop is broken, i.e., we go to Step 3.

Step 2.7. If the excitation is dissipated, the loop is broken, i.e., we go to Step 3.

We are grateful to Felipe Caycedo, Luis Quiroga, and Ferney Rodriguez for earlier discussions about this work.

F.F. thanks Comisión Nacional de Investigación Científica y Tecnológica (Chile) for financial support. A.O.-C. acknowledges funding from Trinity College Oxford (UK) and The Engineering and Physical Sciences Research Council (UK).

REFERENCES

1. Vredenberg, W. J., and L. N. M. Duysens. 1963. Transfer of energy from bacteriochlorophyll to a reaction center during bacterial photosynthesis. *Nature*. 197:355–357.
2. Hu, X., T. Ritz, A. Damjanovic, F. Autenrieth, and K. Schulten. 2002. Photosynthetic apparatus of purple bacteria. *Q. Rev. Biophys.* 35:1–62.
3. Cogdell, R. J., A. Gall, and J. Köhler. 2006. The architecture and function of the light-harvesting apparatus of purple bacteria: from single molecules to in vivo membranes. *Q. Rev. Biophys.* 39:227–324.
4. van Amerongen, H., L. Valkunas, and R. van Grondelle. 2000. Photosynthetic Excitons. World Scientific, Singapore.

5. Deisenhofer, J., O. Epp, K. Miki, R. Huber, and H. Michel. 1985. Structure of the protein subunits in the photosynthetic reaction centre of *Rhodopseudomonas viridis* at 3 Å resolution. *Nature*. 318:618–624.
6. Woodbury, N. W., M. Becker, D. Middendorf, and W. W. Parson. 1985. Picosecond kinetics of the initial photochemical electron-transfer reaction in bacterial photosynthetic reaction centers. *Biochemistry*. 24:7516–7521.
7. Martin, J. L., J. Breton, A. J. Hoff, A. Migus, and A. Antonetti. 1986. Femtosecond spectroscopy of electron transfer in the reaction center of the photosynthetic bacterium *Rhodopseudomonas sphaeroides* R-26: direct electron transfer from the dimeric bacteriochlorophyll primary donor to the bacteriopheophytin acceptor with a time constant of 2.8 ± 0.2 psec. *Proc. Natl. Acad. Sci. USA*. 83:957–961.
8. Frenkel, A. 1954. Light-induced phosphorylation by cell-free preparations of photosynthetic bacteria. *J. Am. Chem. Soc*. 76:5568–5569.
9. Bay, Z., and R. M. Pearlstein. 1963. A theory of energy transfer in the photosynthetic unit. *Proc. Natl. Acad. Sci. USA*. 50:1071–1078.
10. Knox, R. S. 1968. On the theory of trapping of excitation in the photosynthetic unit. *J. Theor. Biol*. 21:244–259.
11. Hemenger, R. P., R. M. Pearlstein, and K. Lakatos-Lindenberg. 1972. Incoherent exciton quenching on lattices. *J. Math. Phys*. 13:1056–1063.
12. Pearlstein, R. M. 1982. Exciton migration and trapping in photosynthesis. *Photochem. Photobiol*. 35:835–844.
13. Kudzmauskas, S., L. Valkunas, and A. Y. Borisov. 1983. A theory of excitation transfer in photosynthetic units. *J. Theor. Biol*. 105:13–23.
14. Owens, T. G., S. P. Webb, L. Mets, R. S. Alberte, and G. R. Fleming. 1987. Antenna size dependence of fluorescence decay in the core antenna of photosystem I: estimates of charge separation and energy transfer rates. *Proc. Natl. Acad. Sci. USA*. 84:1532–1536.
15. Kleinherenbrink, F. A. M., G. Deinum, S. C. M. Otte, A. J. Hoff, and J. Amesz. 1992. Energy-transfer from long-wavelength absorbing antenna bacteriochlorophylls to the reaction center. *Biochim. Biophys. Acta*. 1099:175–181.
16. Pullerits, T., and A. Freiberg. 1992. Kinetic model of primary energy transfer and trapping in photosynthetic membranes. *Biophys. J*. 63: 879–896.
17. Scheuring, S., J. Seguin, S. Marco, D. Lévy, B. Robert, et al. 2003. Nanodissection and high-resolution imaging of the *Rhodopseudomonas viridis* photosynthetic core complex in native membranes by AFM. *Proc. Natl. Acad. Sci. USA*. 100:1690–1693.
18. Scheuring, S., J. N. Sturgis, V. Prima, A. Bernadac, D. Lévy, et al. 2004. Watching the photosynthetic apparatus in native membranes. *Proc. Natl. Acad. Sci. USA*. 101:11293–11297.
19. Scheuring, S., and J. N. Sturgis. 2005. Chromatic adaptation of photosynthetic membranes. *Science*. 309:484–487.
20. Bahatyrova, S., R. N. Frese, C. A. Siebert, J. D. Olsen, K. O. van Der Werf, et al. 2004. The native architecture of a photosynthetic membrane. *Nature*. 430:1058–1062.
21. Scheuring, S., and J. N. Sturgis. 2009. Atomic force microscopy of the bacterial photosynthetic apparatus: plain pictures of an elaborate machinery. *Photosynth. Res*. In press.
22. Ritz, T., S. Park, and K. Schulten. 2001. Kinetics of excitation migration and trapping in the photosynthetic unit of purple bacteria. *J. Phys. Chem. B*. 105:8259–8267.
23. Şener, M. K., J. D. Olsen, C. N. Hunter, and K. Schulten. 2007. Atomic-level structural and functional model of a bacterial photosynthetic membrane vesicle. *Proc. Natl. Acad. Sci. USA*. 104:15723–15728.
24. Godik, V. I., and A. Y. Borisov. 1977. Excitation trapping by different states of photosynthetic reaction centers. *FEBS Lett*. 82:355–358.
25. McDermott, G., S. M. Prince, A. A. Freer, A. M. Hawthornthwaite-Lawless, M. Z. Papiz, et al. 1995. Crystal structure of an integral membrane light-harvesting complex from photosynthetic bacteria. *Nature*. 374:517–521.
26. Scheuring, S., J. L. Rigaud, and J. N. Sturgis. 2004. Variable LH2 stoichiometry and core clustering in native membranes of *Rhodospirillum photometricum*. *EMBO J*. 23:4127–4133.
27. Sturgis, J. N., C. N. Hunter, and R. A. Niederman. 1988. Spectra and excitation coefficients of near-infrared absorption bands in membranes of *Rhodobacter sphaeroides* mutants lacking light-harvesting and reaction center complexes. *Photochem. Photobiol*. 48:243–247.
28. Lakowicz, J. R. 2006. Principles of Fluorescence Spectroscopy, 3rd Ed. Springer, New York.
29. Milano, F., A. Agostiano, F. Mavelli, and M. Trotta. 2003. Kinetics of the quinone binding reaction at the QB site of reaction centers from the purple bacteria *Rhodobacter sphaeroides* reconstituted in liposomes. *Eur. J. Biochem*. 270:4595–4605.
30. Gerencsér, L., G. Laczkó, and P. Maróti. 1999. Unbinding of oxidized cytochrome *c* from photosynthetic reaction center of *Rhodobacter sphaeroides* is the bottleneck of fast turnover. *Biochemistry*. 38:16866–16875.
31. Comayras, F., C. Jungas, and J. Lavergne. 2005. Functional consequences of the organization of the photosynthetic apparatus in *Rhodobacter sphaeroides*. II. A study of PufX$^-$ membranes. *J. Biol. Chem*. 280:11214–11223.
32. Osváth, S., and P. Maróti. 1997. Coupling of cytochrome and quinone turnovers in the photocycle of reaction centers from the photosynthetic bacterium *Rhodobacter sphaeroides*. *Biophys. J*. 73:972–982.
33. Allen, J. P., and J. C. Williams. 1995. Relationship between the oxidation potential of the bacteriochlorophyll dimer and electron-transfer in photosynthetic reaction centers. *J. Bioenerg. Biomembr*. 27:275–283.
34. Mascle-Allemand, C., J. Lavergne, A. Bernadac, and J. N. Sturgis. 2008. Organization and function of the *Phaeospirillum molischianum* photosynthetic apparatus. *Biochim. Biophys. Acta*. 1777:1552–1559.
35. Borisov, A. Y., A. M. Freiberg, V. I. Godik, K. K. Rebane, and K. E. Timpmann. 1985. Kinetics of picosecond bacteriochlorophyll luminescence in vivo as a function of the reaction center state. *Biochim. Biophys. Acta*. 807:221–229.
36. Campillo, A. J., R. C. Hyer, T. G. Monger, W. W. Parson, and S. L. Shapiro. 1977. Light collection and harvesting processes in bacterial photosynthesis investigated on a picosecond time scale. *Proc. Natl. Acad. Sci. USA*. 74:1997–2001.
37. Şener, M. K., and K. Schulten. 2005. Physical principles of efficient excitation transfer in light harvesting. *In* Energy Harvesting Materials. World Scientific, Singapore.
38. Hess, S., M. Chachisvilis, K. Timpmann, M. R. Jones, G. J. S. Fowler, et al. 1995. Temporally and spectrally resolved subpicosecond energy transfer within the peripheral antenna complex (LH2) and from LH2 to the core antenna complex in photosynthetic purple bacteria. *Proc. Natl. Acad. Sci. USA*. 92:12333–12337.
39. Timpmann, K., F. G. Zhang, A. Freiberg, and V. Sundström. 1993. Detrapping of excitation energy from the reaction center in the photosynthetic purple bacterium *Rhodospirillum rubrum*. *Biochim. Biophys. Acta*. 1183:185–193.
40. Scheuring, S., and J. N. Sturgis. 2006. Dynamics and diffusion in photosynthetic membranes from *Rhodospirillum photometricum*. *Biophys. J*. 91:3707–3717.
41. Geyer, T., and V. Helms. 2006. Reconstruction of a kinetic model of the chromatophore vesicles from *Rhodobacter sphaeroides*. *Biophys. J*. 91:927–937.
42. Trissl, H. W., C. J. Law, and R. J. Cogdell. 1999. Uphill energy transfer in LH2-containing purple bacteria at room temperature. *Biochim. Biophys. Acta*. 1412:149–172.
43. Paillotin, G. 1976. Capture frequency of excitations and energy transfer between photosynthetic units in the photosystem II. *J. Theor. Biol*. 58:219–235.
44. Paillotin, G. 1976. Movement of excitations in the photosynthetic domains of photosystem II. *J. Theor. Biol*. 58:237–252.
45. Lavergne, J., and H. W. Trissl. 1995. Theory of fluorescence induction in photosystem-II—derivation of analytical expressions in a model including exciton-radical-pair equilibrium and restricted energy-transfer between photosynthetic units. *Biophys. J*. 68:2474–2492.

46. Comayras, F., C. Jungas, and J. Lavergne. 2005. Functional consequences of the organization of the photosynthetic apparatus in *Rhodobacter sphaeroides*. I. Quinone domains and excitation transfer in chromatophores and reaction center antenna complexes. *J. Biol. Chem.* 280:11203–11213.

47. Şener, M. K., J. Hsin, L. G. Trabuco, E. Villa, P. Qian, et al. 2009. Structural model and excitonic properties of the dimeric RC-LH1-PufX complex from *Rhodobacter sphaeroides*. *Chem. Phys.* 357:188–197.

48. Fujii, R., S. Shimonaka, N. Uchida, A. T. Gardiner, R. J. Cogdell, et al. 2008. Construction of hybrid photosynthetic units using peripheral and core antennae from two different species of photosynthetic bacteria: detection of the energy transfer from bacteriochlorophyll-a in LH2 to bacteriochlorophyll-b in LH1. *Photosynth. Res.* 95:327–337.

49. Escalante, M., Y. Zhao, M. J. W. Ludden, R. Vermeij, J. D. Olsen, et al. 2008. Nanometer arrays of functional light harvesting antenna complexes by nanoimprint lithography and host-guest interactions. *J. Am. Chem. Soc.* 130:8892–8893.